Tunable electronic transport properties of silicon-fullerene-linked nanowires: Semiconductor, conducting wire, and tunnel diode

Kengo Nishio,[1,*] Taisuke Ozaki,[2] Tetsuya Morishita,[1] and Masuhiro Mikami[1]

[1]*Research Institute for Computational Sciences (RICS), National Institute of Advanced Industrial Science and Technology (AIST), Central 2, Umezono 1-1-1, Tsukuba, Ibaraki 305-8568, Japan*

[2]*Research Center for Integrated Science (RCIS), Japan Advanced Institute of Science and Technology (JAIST), 1-1 Asahidai, Nomi, Ishikawa 923-1292 Japan*

(Received 8 December 2009; revised manuscript received 28 January 2010; published 24 March 2010)

We explore the possibility of controllable tuning of the electronic transport properties of silicon-fullerene-linked nanowires by encapsulating guest atoms into their cages. Our first-principles calculations demonstrate that the guest-free nanowires are semiconductors, and do not conduct electricity. The iodine or sodium doping improves the transport properties, and makes the nanowires metallic. In the junctions of I-doped and Na-doped NWs, the current travels through the boundary by quantum tunneling. More significantly, the junctions have asymmetric I-V_b curves, which could be used as rectifiers. The current-voltage curves are interpreted by band-overlapping models. Tunable electronic transport properties of silicon-fullerene-linked nanowires could find many applications such as field-effect transistors, conducting wires, and tunnel diodes.

DOI: 10.1103/PhysRevB.81.115444 PACS number(s): 73.21.Hb, 73.22.−f, 73.61.Wp, 73.63.Nm

I. INTRODUCTION

Silicon nanowires (Si NWs) have attracted much attention because of the potential uses in widespread applications, including microelectronics,[1,2] solar energy,[3,4] and biomedical technologies.[5] Precise tuning of their physical properties is crucial to the application of Si NWs. So far, bulklike Si NWs which adopt the diamond structure have been studied extensively. Experimental measurements have demonstrated that the current bias voltage (I-V_b) curves of Si NWs can be tuned by substitutional doping of boron and phosphorous.[2] Computational studies have demonstrated that the crystal orientation of nanowire affects the effective masses of carriers[6] and the I-V_b curve.[7–9] The band gap energy of Si NWs increases as the size decreases due to the quantum-confinement effect.[10,11] Such crystal-orientation and quantum-confinement effects will be utilized to tailor their physical properties as far as Si NWs adopt the diamond structure.

The most stable structure of bulk Si is the diamond structure. The diameter of bulklike Si NWs can be reduced to below 3 nm by etching bulk Si or large-diameter Si NWs.[12,13] On the other hand, the diamond structure is predicted to be no longer the most stable for Si NWs with diameters below 6 nm.[14–19] This prediction indicates a possibility that nonbulklike Si NWs which adopt structures other than the diamond structure can be synthesized if appropriate growth techniques are used.

To establish controllable growth techniques of Si nanostructures, much computational effort has been devoted.[17–22] Recent molecular-dynamics simulations have demonstrated that liquid Si confined in a cylindrical nanopore crystallizes into a polyicosahedral nanowire composed of icosahedral Si nanodots, or multishell Si fullerenes $Si_{20}@Si_{80}$.[17,19] It has also been demonstrated that Si_{16}- and Si_{20}-linked NWs can be synthesized by using carbon nanotubes of appropriate diameters as template.[18,19] The change in their atomic structure would expand the range of Si NW application because the physical properties of nonbulklike Si NWs are expected to be dramatically different from the bulklike ones.[19,23] Moreover, the unique cage structure of silicon-fullerene-linked NWs provides an opportunity to tune their physical properties by encapsulating guest atoms into the cages.

First-principles calculations have demonstrated that the band structures of Si-fullerene-linked NWs can be tuned from semiconducting to metallic by the guest atom encapsulation.[18,19,24] It has also been demonstrated that the transmission curve at zero bias is tunable.[25] However, a recent first-principles study has warned that the metallic band structure and nonzero transmission at zero bias are not enough to conclude that the material conducts electricity.[26,27] Calculations under bias are therefore desirable.

In this paper, we study the effects of iodine and sodium encapsulation on the I-V_b curves of hydrogen-terminated Si_{16}- and Si_{20}-linked NWs by means of first-principles calculations. Our results demonstrate that the guest-free nanowires are semiconductors, and do not conduct electricity. The iodine or sodium doping improves the transport properties, and makes the nanowires metallic. We further demonstrate that the junctions of I-doped NWs and Na-doped NWs have asymmetric I-V_b curves, which could be used as rectifiers.

II. COMPUTATIONAL DETAILS

A. Electronic structure and transport calculations

We calculated the electronic structure of Si-fullerene-linked NWs under bias voltage by a combination of the nonequilibrium Green's function (NEGF) method[28–33] and the density functional theory (DFT) (Refs. 34 and 35) within the local density approximation (LDA).[36,37] The method has been widely applied to study the electronic transport properties of nanosized materials.[7,8,26,33,38,39]

The continued fraction representation of the Fermi-Dirac function[33,40] was used to carry out the contour integration in the calculation of the equilibrium density matrix. On the other hand, nonequilibrium density matrix was calculated by

numerical integration along a line close to the real axis.[33]

Norm-conserving pseudopotentials were used in a separable form with multiple projectors to replace the deep core potential into a shallow potential.[41,42] The wave functions were expressed by the linear combination of atomic orbitals centered on atomic sites. The atomic basis functions were generated by solving atomic Kohn-Sham equations using confinement pseudopotentials.[43,44] The primitive pseudoatomic basis sets, Si6.5-$s2p2d1$, H5.5-$s2$, I8.0-$s2p1$, and Na8.0-s1$p1d1$, were used for Si, H, I, and Na atoms, respectively. Here, the abbreviation, for example Si6.5-$s2p2d1$, represents the employment of two primitive s orbitals, two primitive p orbitals, and one primitive d orbital of a Si atom, which were generated with a confinement radius 6.5 Bohr. The real space grid techniques were used with the cutoff energy of about 120 Ry, when calculating Hamiltonian matrix elements and solving the Poisson equation with a fast Fourier transformation.[45]

We calculated the current using the Landauer formula,[28,29,46]

$$I(V_b) = \frac{2e}{h}\int T(E)\Delta f(E)dE, \tag{1}$$

$$V_b = \frac{\mu_r - \mu_l}{e}, \tag{2}$$

and

$$\Delta f(E) = f(E-\mu_r) - f(E-\mu_l). \tag{3}$$

Here, V_b is the applied bias voltage, 2 comes from the spin multiplicity, e is the electron charge, h is the Planck constant, $T(E)$ is the transmission curve, μ_l and μ_r are the chemical potentials of left and right electrodes, respectively, and $f(E)$ is the Fermi-Dirac function. The transmission curve is defined as

$$T(E) = \mathrm{Tr}[\mathrm{Im}\{\Sigma_L(E)\}G_C^r(E)\mathrm{Im}\{\Sigma_R(E)\}G_C^a(E)], \tag{4}$$

where $G_C^{r/a}(E)$ is the retarded/advanced Green's function matrix of the central scattering region and $\Sigma_{L/R}(E)$ is the self-energy matrix of the left (L)/right (R) electrode. All the calculations were carried out using the OPENMX code.[47]

B. band-overlapping model

The transmission curve, in principle, can be decomposed into the contributions as

$$T(E) = \sum_{i(l),j(r)} T_{i(l)j(r)}(E), \tag{5}$$

where the $T_{i(l)j(r)}(E)$ is the contribution from the $i(l)$ band of the left electrode and $j(r)$ band of the right electrode. The pair of the $i(l)$ and $j(r)$ bands can be classified into the allowed or prohibited pairs according to the symmetries of wave functions.[26,27,38] When the bands of the allowed pair overlap each other in energy, the transmission channel is open. If the electron does not experience the scattering in the scattering region, the allowed pair contributes to the transmission curve by one in the overlapping energy range where the bands overlap each other. But, in general, the scattering reduces the efficiency of the channel, and the contribution to the transmission curve is reduced from one. The current also can be decomposed into the contributions as

$$I(V_b) = \sum_{i(l),j(r)} I_{i(l)j(r)}(V_b), \tag{6}$$

where

$$I_{i(l)j(r)}(V_b) = \frac{2e}{h}\int T_{i(l)j(r)}(E)\Delta f(E)dE. \tag{7}$$

Evaluating each contribution is helpful to interpret the I-V_b curve. However, it is difficult for the NEGF calculation alone. In order to complement the NEGF calculation, we introduce a band-overlapping (BO) model which reproduces the transmission curve and the I-V curve in terms of the band overlapping as follows.

In the BO model, we first classify $i(l)j(r)$ pairs into allowed or prohibited pairs. However, the direct examination from the wave function symmetries is difficult, because the wave functions are related to the transmission curve via the Green's functions and self-energies in a complicated manner [Eq. (4)]. Therefore, we determine the selection rule on the basis of careful comparison between the transmission curve and the energy range where the $i(l)$ and $j(r)$ bands overlap each other. In the comparison, we pay particular attention at the edges of the overlapping energy range, where the transmission curve should show steep changes if the pair is allowed. For allowed pairs, we ignore the scattering effects in the overlapping energy range. Namely, the contribution to the transmission curve is assumed as

$$T_{i(l)j(r)}(E) = \begin{cases} 1 & (E \subseteq E_{\mathrm{overlapping}}) \\ 0 & (\mathrm{otherwise}) \end{cases}, \tag{8}$$

where $E_{\mathrm{overlapping}}$ is the overlapping energy range. For prohibited pairs,

$$T_{i(l)j(r)}(E) = 0. \tag{9}$$

We evaluate the contribution to the current as

$$I_{i(l)j(r)}(V_b) = \frac{2e}{h}\int_{\mu_l}^{\mu_r} T_{i(l)j(r)}(E)dE. \tag{10}$$

Here, the temperature of the Fermi-Dirac function in Eq. (7) is set zero to make the current variation clear. The BO model reproduces the NEGF calculation well when the scattering effects are small as we will see later.

Note that we will use abbreviations $I_{\mathrm{NEGF}}/T_{\mathrm{NEGF}}$ and $I_{\mathrm{BO}}/T_{\mathrm{BO}}$ to distinguish the current/transmission curve obtained by the NEGF calculation and that obtained by the BO model, as necessary.

C. Structure optimization

The Si_{16}-linked NW studied here is constructed by linking Si_{16} fullerene cages together.[18,19] The constituent Si_{16} cage has two square faces and eight pentagonal faces. Adjacent Si_{16} cages are linked together by sharing one square face.

Similarly, the Si_{20}-linked NW is constructed by linking Si_{20} fullerene cages together.[14,18,19] The constituent Si_{20} cage has 12 pentagonal faces. Adjacent Si_{20} cages are linked together by sharing one pentagonal face. We terminated all the surface dangling bonds by hydrogen atoms. Si atoms in the Si-fullerene-linked NWs are joined by tetrahedral sp^3 bonding as the conventional bulk diamond Si. However, the tetrahedral network structures of the Si-fullerene-linked NWs are completely different.

The model used to study the electronic transport consists of three regions: left electrode, scattering region, and right electrode. As an example, the model for the junction of an I-doped Si_{16}-linked NW and a Na-doped Si_{16}-linked NW is shown in Fig. 1(a). The self-electrode model was used; the semi-infinite left (right) electrode is the same material as the right (left) end of the central scattering region. The model was prepared as follows.

We first optimized the structures of the infinite I-doped Si_{16}-linked NW ($I_2@Si_{24}H_{16}$ NW) and the infinite Na-doped Si_{16}-linked NW ($Na_2@Si_{24}H_{16}$ NW) until the force of each atom becomes 0.0001 hartree/bohr or less by the conventional band structure calculation. The optimized I-doped Si_{16}-linked NW is depicted in Fig. 1(c). The optimized length of a unit cell in the wire direction was determined by comparing total energies calculated with different cell lengths. The semi-infinite electrodes used in the NEGF calculation are assumed to have the same atomic structures as the corresponding infinite nanowires obtained through above procedure.

We then optimized the structure of the scattering region with a cluster model [Fig. 1(b)]. The cluster consists of three parts: left-buffer, boundary, and right-buffer parts. The boundary part contains the boundary between the Na-doped NW and the I-doped NW, and was relaxed during the optimization process. The left-buffer and right-buffer parts contain the same atomic structures as the infinite I-doped Si_{16}-linked NW and the infinite Na-doped Si_{16}-linked NW, respectively, and were fixed during the optimization process. We terminated dangling bonds of Si atoms at both ends of the cluster by hydrogen atoms, which were removed after the optimization process. We connected the optimized cluster to the left and right electrodes. The electrodes are smoothly connected to the cluster because left-buffer and right-buffer parts have the same atomic structures as the left and right electrodes, respectively.

We note that electrons near the boundary would transfer from the Na-doped NW to the I-doped NW, forming the depletion region, or the insulating region, near the boundary. If the length of the insulating region is short enough, the current travels through the boundary by quantum tunneling. The size of scattering region might affect the length of the depletion region. The larger size is desirable, but limited by computational resources. In order to check that our model is large enough, we investigate the electronic charge transfer in a heterogeneously doped Si_{16}-linked cluster, $I_{14}Na_{14}@Si_{340}H_{232}$. The cluster is constructed by linking 14 $I@Si_{16}$ cages and fourteen $Na@Si_{16}$ cages, and all the dangling bonds are terminated by hydrogen atoms. We measure the charge transfer by a partial charge difference ΔQ of the $G@Si_{16}H_8$ cage defined as

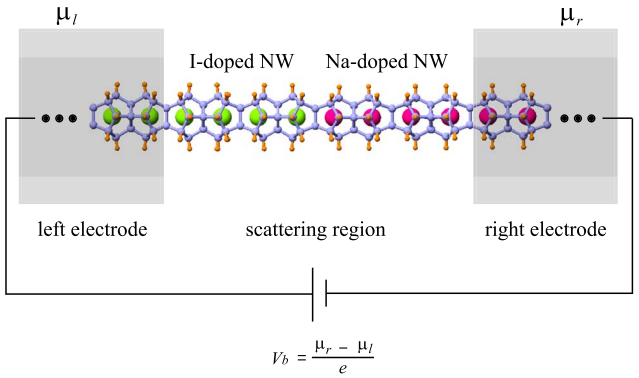

(a) junction of I-doped and Na-doped Si_{16}-linked NWs

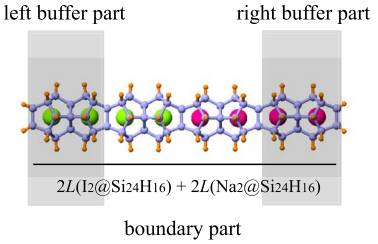

(b) cluster used to optimize atomic structure near the boundary

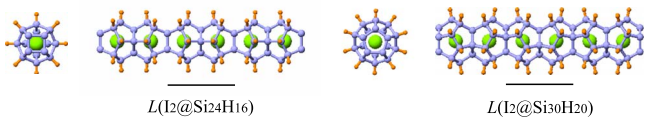

(c) $I_2@Si_{24}H_{16}$ NW (d) $I_2@Si_{30}H_{20}$ NW

FIG. 1. (Color online) (a) Model used to study the electronic transport in the junction of an I-doped Si_{16}-linked NW and a Na-doped Si_{16}-linked NW. Small, medium, large light-gray (green), and large gray (purple) particles represent H, Si, I, and Na atoms, respectively. The electrodes are shaded. The chemical potentials of the left and right electrodes are assumed to be μ_l and μ_r, respectively. The bias voltage V_b is defined as $V_b=(\mu_r-\mu_l)/e$, where e is the electron charge. (b) Cluster model used to optimize the structure near the boundary between the I-doped and Na-doped Si_{16}-linked NWs. The horizontal bar represents the distance between the two square atomic rings, $2L(I_2@Si_{24}H_{16})+2L(Na_2@Si_{24}H_{16})$, where $L(I_2@Si_{24}H_{16})$ and $L(Na_2@Si_{24}H_{16})$ are the unit cell lengths of the $I_2@Si_{24}H_{16}$ NW and the $Na_2@Si_{24}H_{16}$ NW, respectively. (c) Structure of I-doped Si_{16}-linked NW ($I_2@Si_{24}H_{16}$ NW). The horizontal bar represents the length of the unit cell in the wire direction. (d) Structure of I-doped Si_{20}-linked NW ($I_2@Si_{30}H_{20}$ NW). The horizontal bar represents the length of the unit cell in the wire direction.

$$\Delta Q = \frac{1}{2}\sum_{i=1}^{4}\Delta q_{\mathrm{Si}}(i) + \sum_{i=5}^{12}\Delta q_{\mathrm{Si}}(i) + \frac{1}{2}\sum_{i=13}^{16}\Delta q_{\mathrm{Si}}(i) + \sum_{i=1}^{8}\Delta q_{\mathrm{H}}(i) + \Delta q_{\mathrm{G}}, \tag{11}$$

where

$$\Delta q_X(i) = m_X(i) - a_X, \tag{12}$$

$m_X(i)$ is the Mulliken charge of the ith X atom, and a_X is the charge of an isolated X atom. Si atoms of $i=1-4$ and 13–16

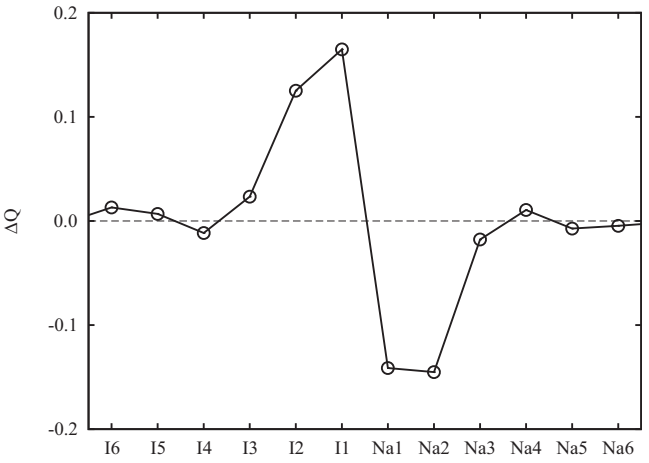

FIG. 2. Partial charge differences of $I@Si_{16}H_8$ and $Na@Si_{16}H_8$ cages of the $I_{14}Na_{14}@Si_{340}H_{233}$ cluster. The notation I*i*/Na*i* indicates the *i*th $I@Si_{16}H_8$/$Na@Si_{16}H_8$ cage numbering from the boundary.

are atoms of square rings. One square ring is shared by two $G@Si_{16}H_8$ cages. Therefore, we assumed that half of the charges on the square ring belongs to one cage, and the other half belongs to the other cage. Figure 2 shows how the $\Delta Q(Ii)/\Delta Q(Nai)$ decays as the distance from the boundary increases, where I*i*/Na*i* means the *i*th $I@Si_{16}H_8$/$Na@Si_{16}H_8$ cage numbering from the boundary. The electron transfer mainly occurs between two $I@Si_{16}H_8$ cages and two $Na@Si_{16}H_8$ cages near the boundary. Therefore, the size of scattering region composed of four $I@Si_{16}H_8$ cages and four $Na@Si_{16}H_8$ cages is reasonable.

III. RESULTS

A. Guest-free Si_{16}-linked NW

The hydrogen-terminated guest-free Si_{16}-linked NW does not conduct electricity in the range of bias voltage from −1 to 1 V [Fig. 3(a)] because the nanowire is a semiconductor with a 2.29 eV band gap [Fig. 4(a)].

B. I-doped Si_{16}-linked NW

The encapsulation of I atoms into the Si_{16} cages improves the electronic transport property of the nanowire. Although the structure deformation and orbital hybridization somewhat affect the band structure of the nanowire, the most important effect of the iodine doping is the electron transfer from the Si NW to the I atoms due to the greater electronegativity of iodine. The electron transfer results in partially empty valence bands of the Si NW, and the I-doped Si_{16}-linked NW is a metal [Fig. 4(b)].

The I-V_b curve of the I-doped Si_{16}-linked NW is given in Fig. 3(a). The curve is symmetric, $I(V_b)=-I(-V_b)$, because the left electrode, scattering region, and right electrode are made of the same material. We therefore discuss only the current under positive bias. The current first increases linearly as the bias voltage is applied. The slope dI/dV_b is about $2G_0$, where G_0 is the quantum conductance $2e^2/h$. The

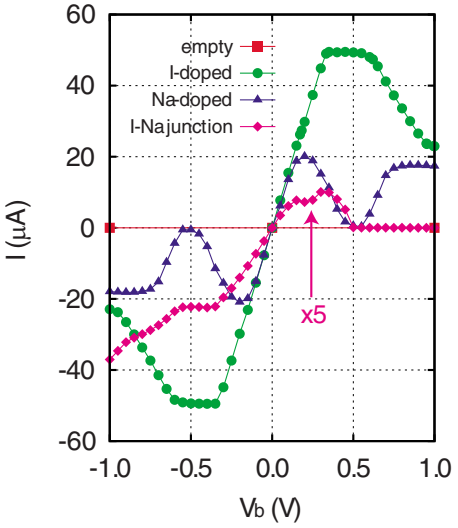

(a) Si16-linked NWs

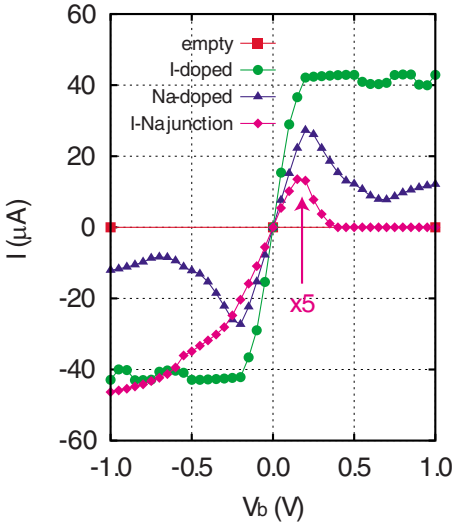

(b) Si20-linked NWs

FIG. 3. (Color online) $I-V_b$ curves for (a) Si_{16}-linked NWs and (b) Si_{20}-linked NWs. Squares, circles, triangles, and diamonds are results for guest-free NW, I-doped NW, Na-doped NW, and the junction of the I-doped NW and the Na-doped NW, respectively. The currents in the I-Na junctions are magnified five times for clarity.

current then becomes almost bias independent at around 0.35 V, and starts to decrease with a slope of about $-G_0$ at around 0.55 V.

In order to better understand the I-V_b curve, we use a BO model. Figure 5(a) shows the band structure near the Fermi energy. By carefully comparing the transmission curve and the band structures of the left and right electrodes at bias voltages from 0 to 1 V (see Appendix A), we find that only the red (r) and blue (b) bands contribute to the transmission curve in the transport energy range, which is the energy range from μ_l to μ_r. We also find that $r(l)r(r)$ and $b(l)b(r)$ pairs are allowed, and that $r(l)b(r)$ and $b(l)r(r)$ pairs are

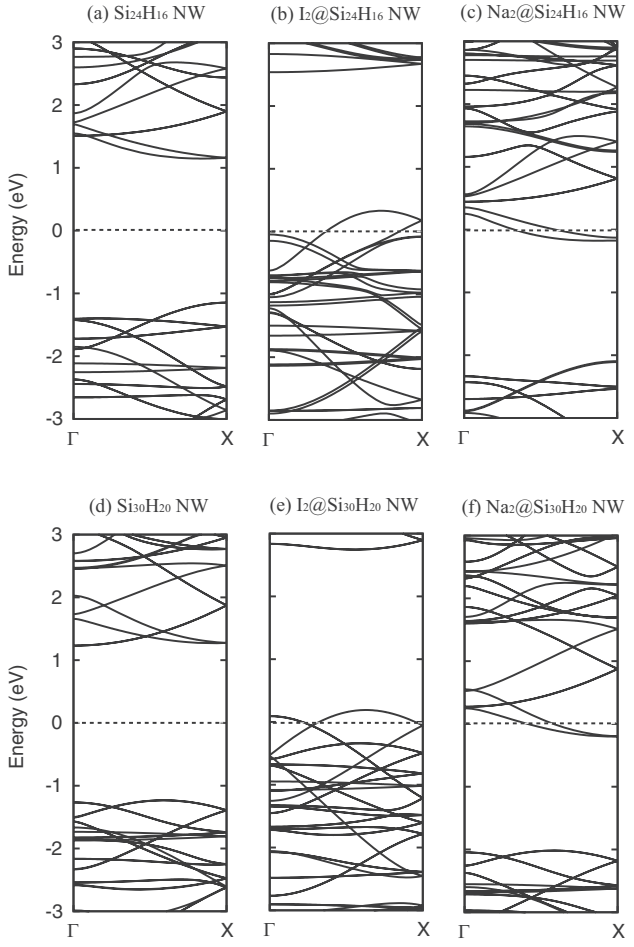

FIG. 4. Band structures of infinite Si-fullerene-linked NWs. (a) guest-free, (b) I-doped, and (c) Na-doped Si_{16}-linked NWs. (d) guest-free, (e) I-doped, and (f) Na-doped Si_{20}-linked NWs. The energy is measured from the Fermi energy shown by the dashed horizontal line.

prohibited. The other bands could contribute considerably to the transmission outside the transport energy range. However, such transmission does not contribute to the current. We therefore need not to take account of the effects of the other bands. Note that the α and β bands are shown by the dashed and dash-dotted lines, respectively. The r band is part of the α band from the Γ point to the T point ($\alpha_{\Gamma T}$), where the T point corresponds to the top of the α band. The α_{TX} and β bands are continually joined to form the b band with a small energy gap of 0.010 eV at the X point.

Figure 5(b) shows that the BO model reproduces the overall shape of the I-V_b curve obtained by the NEGF calculation well. The BO model also reproduces the transmission curve well [Fig. 5(c)]. The current I_{BO} is given by the summation of the $I_{r(l)r(r)}$ and $I_{b(l)b(r)}$. Generally, each contribution has three regions: the increasing current region with a slope of G_0, constant current region, and decreasing current region with a slope of $-G_0$.

The shape of the I_{BO}-V curve is explained in terms of decomposed currents as follows. The increase in the current from 0.00 to 0.332 V arises from the increase in the $I_{r(l)r(r)}$ and $I_{b(l)b(r)}$. The slope is therefore $2G_0$, except for G_0 in a narrow bias-voltage range from 0.172 to 0.182 V, where the chemical potential of the right electrode μ_r is passing through the energy gap between the $\alpha_{TX}(l)$ and $\beta(l)$ bands. All the contributions, thus the current, become constant at 0.332 V, where the chemical potential of the right electrode μ_r exceeds the tops of the $r(l)$ and $b(l)$ bands. The current starts to decrease with a slope of $-G_0$ at 0.621 V, where the bottom of the $r(r)$ band exceeds the chemical potential of the left electrode μ_l and the $I_{r(l)r(r)}$ starts to decrease. The contribution $I_{r(l)r(r)}$ reaches zero at 0.953 V, where the bottom of the $r(r)$ band exceeds the top of the $r(l)$ band. Only the $I_{b(l)b(r)}$ contributes to the current above 0.953 V. The current starts to decrease with a slope of $-G_0$ at 0.995 V, where the bottom of the $b(r)$ band exceeds the chemical potential of the left electrode μ_l and the $I_{b(l)b(r)}$ starts to decrease.

The overall shape of the I_{NEGF}-V_b curve is explained by the band overlapping, because the NEGF calculation and BO model coincide well. But there are some minor discrepancies between the I_{NEGF} and I_{BO}, which stem from our assumption on the $T_{i(l)j(r)}(E)$. Namely, we ignored the scattering effects in the energy range where the $i(l)$ and $j(r)$ bands overlap each other. This assumption is true at zero bias voltage. However, under finite bias voltage, the scattering reduces the $T_{i(l)j(r)}$ from one, and the effect is prominent near the energies corresponding to band edges [Fig. 5(c)]. Consequently, the BO model somewhat overestimates the current, and the I_{NEGF}-V_b curve is smoother than the I_{BO}-V_b curve.

C. Na-doped Si_{16}-linked NW

The encapsulation of Na atoms into the Si_{16} cages also makes the nanowire metallic. However, the mechanism is the opposite of the I-doping. In the Na-doped NW, electrons are transferred from Na atoms to the Si NW due to the greater electropositivity of sodium. The conduction bands of the Si NW are therefore partially filled, and the Na-doped Si_{16}-linked NW is a metal [Fig. 4(c)].

The I-V_b curve of the Na-doped Si_{16}-linked NW is similar to that of the I-doped Si_{16}-linked NW in the low bias-voltage range [Fig. 3(a)], because the numbers of crossing points where the bands intersects the Fermi energy are the same. However, the overall shapes of the I-V_b curves are dramatically different. Actually, the current in the Na-doped Si_{16}-linked NW first increases, then decreases to almost zero at around 0.5 V, and increases again, as the positive bias voltage is applied.

In order to better understand the I-V_b curve, we use a BO model. Figure 6(a) shows the band structure of the Na-doped Si_{16}-linked NW near the Fermi energy. By carefully comparing the transmission curve and the band structures of the left and right electrodes at bias voltages from 0 to 1 V (see Appendix B for some comparisons), we find that only the green (g), orange (o), cyan (c), magenta (m), and black-dashed bands contribute to the transmission curve in the transport energy range. We ignore the effect of the black-dashed band, because the band width is narrow and the contribution to the current is negligible. We also find that $g(l)g(r)$, $o(l)o(r)$, and $[c(l),m(l)][g(r),o(r)]$ pairs are allowed, and that the $g(l)o(r)$ and $o(l)g(r)$ pairs are prohibited. Here, we use an abbreviation,

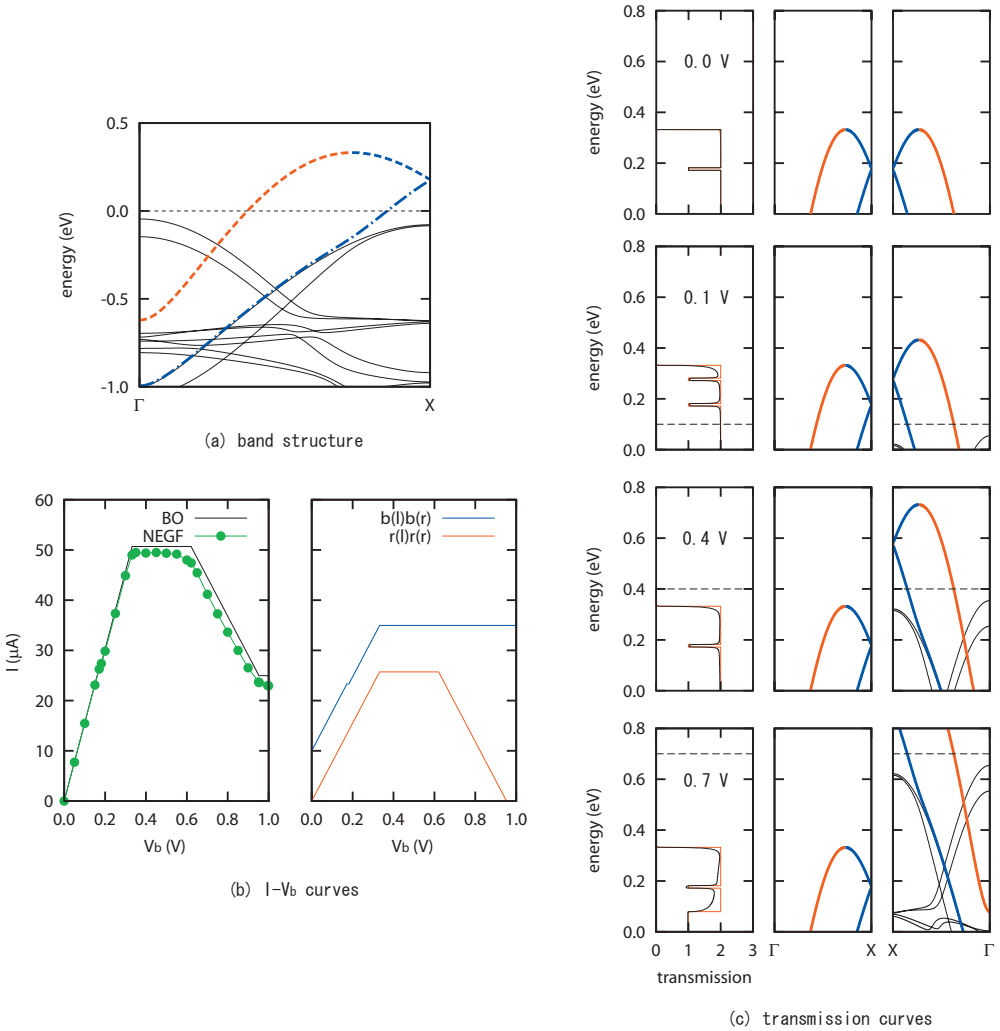

FIG. 5. (Color) Band-overlapping model for I-doped Si_{16}-linked NW. (a) Band structure near the Fermi energy. The energy is measured from the Fermi energy shown by the horizontal short dashed line. The α band is drawn by the dashed line. The red and blue dashed lines are the $\alpha_{\Gamma T}$ and α_{TX} bands, respectively. The β band is drawn by the dash-dotted line. (b) I-V_b curves. The curves obtained by the BO model and NEGF calculation are given in the left. The contributions, $I_{b(l)b(r)}$ and $I_{r(l)r(r)}$, are given in the right. The $I_{b(l)b(r)}$ is shifted upward by 10 μA for clarity. (c) Transmission curves, band structures of the left electrode, and band structures of the right electrode are given in the left, middle, and right, respectively. The energy is measured from the chemical potential of the left electrode μ_l. The chemical potential of the right electrode μ_r is shown by the dashed line. The results of 0.0, 0.1, 0.4, and 0.7 V are given in the upper, upper-middle, lower-middle, and lower rows, respectively. The transmission curves obtained by the BO model and NEGF calculations are shown by the red and black lines, respectively.

$$[c(l),m(l)][g(r),o(r)] = c(l)g(r),c(l)o(r),m(l)g(r),m(l)o(r). \tag{13}$$

We need not to take account of the other pairs, because they do not contribute to nonzero values of the transmission curve in the transport energy range. Note that the γ band is shown by the dashed line. The g band is part of the γ band from the Γ point to the B point ($\gamma_{\Gamma B}$), where the B point corresponds to the bottom of the γ band. The black-dashed band is the γ_{BX} band.

Figure 6(b) shows that the BO model qualitatively reproduces the overall shape of the I-V_b curve obtained by the NEGF calculation. Therefore, the I_{NEGF}-V_b curve is explained by the I_{BO}-V_b curve. The I_{BO}-V_b curve has three regions: the low-bias conducting region below 0.482 V, insulating region from 0.482 to 0.532 V, and high-bias conducting region above 0.532 V. Figure 6(b) shows that the I_{BO} below 0.482 V comes from the $I_{g(l)g(r)}$ and $I_{o(l)o(r)}$, and the I_{BO} above 0.532 V comes from the $I_{[c(l),m(l)][g(r),o(r)]}$, where

$$I_{[c(l),m(l)][g(r),o(r)]} = I_{c(l)g(r)} + I_{c(l)o(r)} + I_{m(l)g(r)} + I_{m(l)o(r)}. \tag{14}$$

The insulating region occurs because of the energy gap between the g and c bands and the energy gap between the o and c bands. We note that the BO model considerably overestimates the current above 0.5 V and the T_{NEGF} is less than half of the T_{BO} in the energy range where the transmission comes from the $[c(l),m(l)][g(r),o(r)]$ pairs [Fig. 6(c)]. This

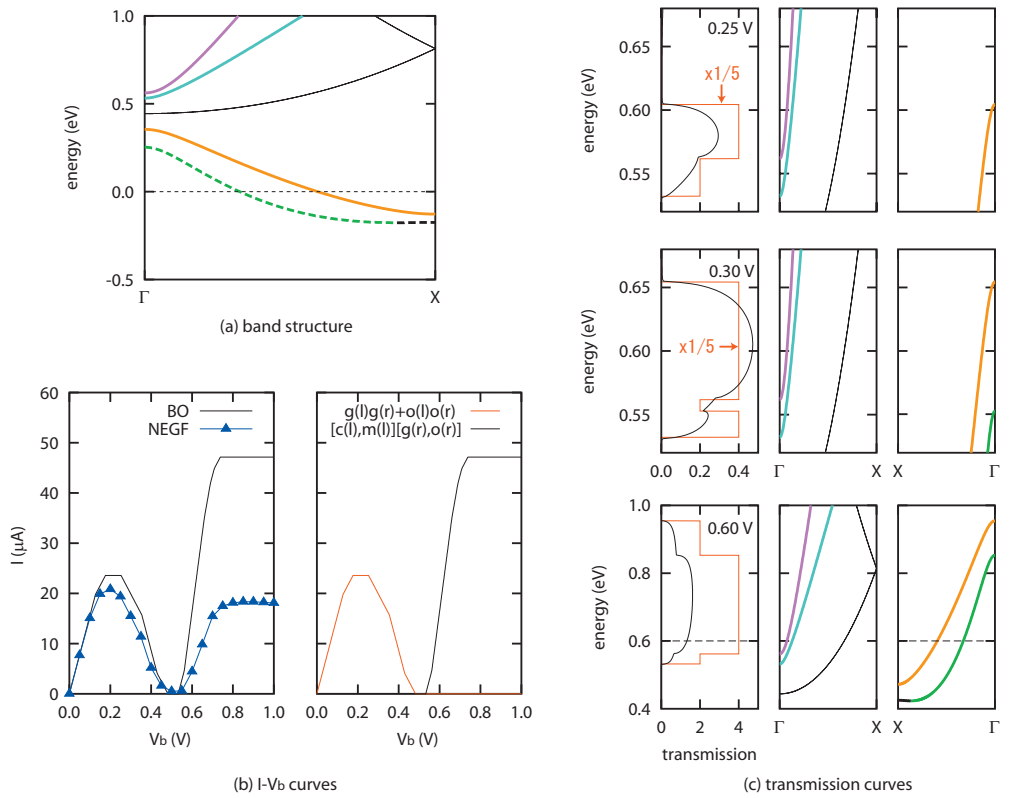

FIG. 6. (Color) Band-overlapping model for Na-doped Si_{16}-linked NW. (a) band structure near the Fermi energy. The energy is measured from the Fermi energy shown by the horizontal short dashed line. The γ band is drawn by the dashed line. The green and black dashed lines are the $\gamma_{\Gamma B}$ and γ_{BX} bands, respectively. (b) I-V_b curves. The curves obtained by the BO model and NEGF calculation are given in the left. The contributions, $I_{g(l)g(r)}+I_{o(l)o(r)}$ and $I_{[c(l),m(l)][g(r),o(r)]}$, are given in the right. (c) Transmission curves, band structures of the left electrode, and band structures of the right electrode are given in the left, middle, and right, respectively. The energy is measured from the chemical potential of the left electrode μ_l. The chemical potential of the right electrode μ_r is shown by the dashed line. The results of 0.25, 0.30, and 0.60 V are given in the upper, middle, and lower rows, respectively. The transmission curves obtained by the BO model and NEGF calculation are shown by the red and black lines, respectively. Note that the 1/5 of T_{BO} is given at 0.25 and 0.30 V for clarity.

means that the scattering effects are nontrivial for the $[c(l),m(l)][g(r),o(r)]$ pairs.

D. Junction of the I-doped and Na-doped Si_{16}-linked NWs

The I-V_b curve of the junction of the I-doped and Na-doped Si_{16}-linked NWs, or a heterogeneously doped NW, is dramatically different from that of the homogeneously doped NWs. Actually, the junction functions as tunnel diode. When the positive bias is applied, the current first increases, but it starts to decrease at 0.3 V, and eventually becomes almost zero above 0.5 V. In contrast, when the negative bias is applied, the current keeps increasing.

In order to understand the mechanism of the asymmetric I-V_b curve, we use a BO model. Here, we consider only the area where the density of states (DOS) of the left electrode (I-doped NW) overlaps with the DOS of the right electrode (Na-doped NW). The left electrode does not have the electronic states slightly above the Fermi energy, while the right electrode does not have slightly below the Fermi energy. This opposite nature of DOSs is key for the asymmetric I-V_b curve of the I-Na junction as follows. When the positive bias is applied, the overlapping area first increases, but starts to decrease at 0.332 V, where the chemical potential of the right electrode μ_r exceeds the top of the $\alpha(l)$ band (Fig. 7). Eventually, the overlapping area disappears at 0.509 V, where the bottom of the $\gamma(r)$ band exceeds the top of the $\alpha(l)$ band. According to the variations in the overlapping area in the transport energy range, the current first increases, and then decreases to almost zero. In contrast, when the negative bias is applied, the overlapping area in the transport energy range keeps increasing, and the current keeps increasing.

The current flows in the I-Na junction, but smaller than the metallic Na-doped and I-doped NWs. This is because the current travels through the boundary between the I-doped and Na-doped NWs by quantum tunneling as heavily doped p-n junctions of bulk semiconductors.[48,49] Actually, partial DOSs (PDOSs) of $G@Si_{16}H_8$ cages at zero bias voltage shows that PDOSs of cages forming boundary, PDOS(I1) and PDOS(Na1), are considerably small near the Fermi energy (Fig. 8).

E. Si_{20}-linked NWs

The effects of iodine and sodium doping on the electronic transport properties of the Si_{20}-linked NWs are essentially the same as the Si_{16}-linked NWs; the semiconducting guest-free NW becomes metallic by I or Na doping, and the junc-

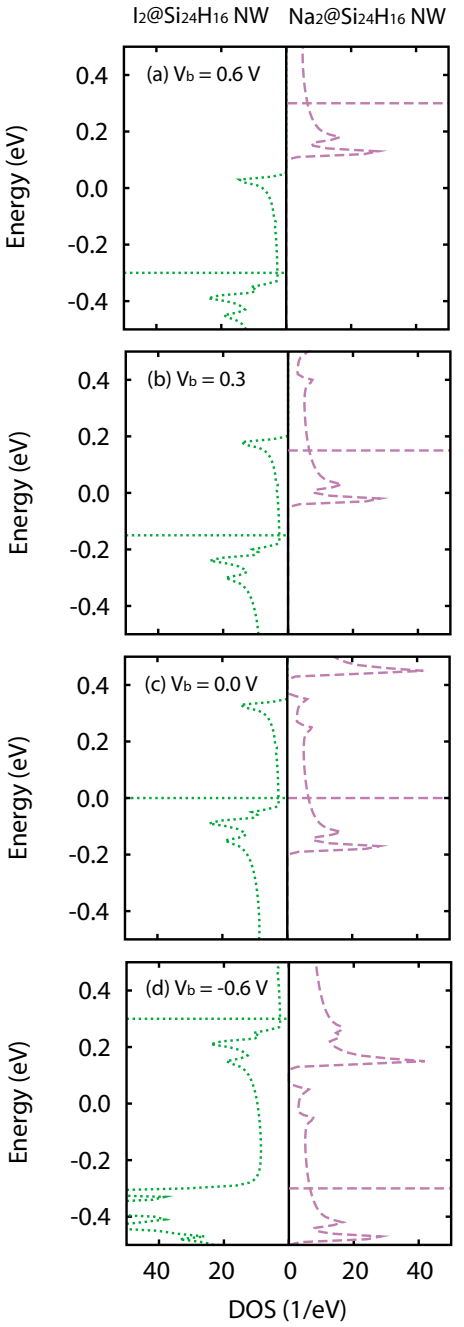

FIG. 7. (Color online) Overlapping area of DOSs. The dotted line is the DOS of the left electrode (I-doped Si_{16}-linked NW), while the dashed line is the DOS of the right electrode (Na-doped Si_{16}-linked NW). (a) V_b=0.6 V, (b) 0.3 V, (c) 0.0 V, and (d) −0.6 V. Horizontal bars represent the chemical potentials of the left and right electrodes. The energy is measured from $(\mu_l+\mu_r)/2$.

tion of the I-doped and Na-doped NWs has an asymmetric *I-V* curve. However, some notable differences are observed in I-doped NWs and Na-doped NWs.

The I-doped Si_{20}-linked NW conducts more electricity than the I-doped Si_{16}-linked NW at low bias voltage. This is because the higher number of crossing points, 4: the red (r), blue (b), and twofold-degenerated green (g) bands cross the Fermi energy [Fig. 9(a)]. The I-V_b curve of the I-doped Si_{20}-linked NW does not have current-decreasing region in

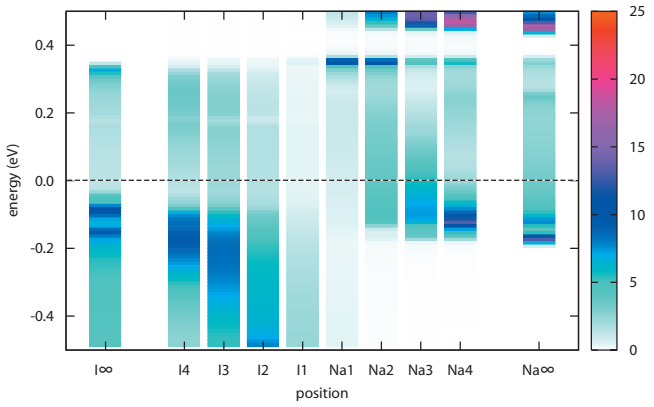

FIG. 8. (Color) Map of PDOSs of $I@Si_{16}H_8$ and $Na@Si_{16}H_8$ cages of the junction of I-doped and Na-doped Si_{16}-linked NWs at zero bias. PDOSs are depicted in arbitrary unit. The notation Ii/Nai indicate the ith $I@Si_{16}H_8$/$Na@Si_{16}H_8$ cage numbering from the boundary. PDOSs at I∞ and Na∞ correspond to PDOSs of the infinite I-doped and Na-doped Si_{16}-linked NWs, respectively.

the bias-voltage range we studied, except for two dips around 0.625 and 0.925 V. Our BO analysis explained the I-V_b curve as follows. The current is given by the summation of the contributions from $r(l)r(r)$, $b(l)b(r)$, and $g(l)g(r)$

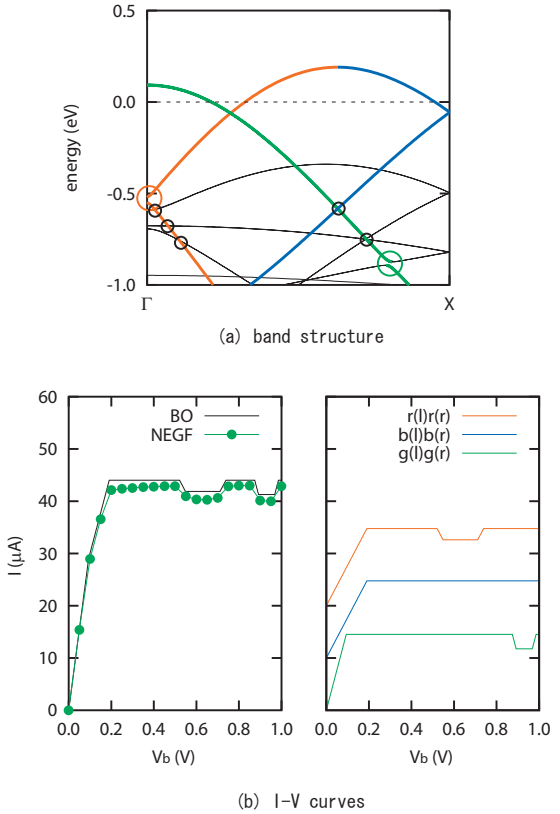

FIG. 9. (Color) Band-overlapping model for I-doped Si_{20}-linked NW. (a) band structure near the Fermi energy. The energy is measured from the Fermi energy shown by the horizontal dashed line. (b) I-V_b curves. The curves obtained by the BO model and NEGF calculation are given in the left. The contributions, $I_{r(l)r(r)}$, $I_{b(l)b(r)}$ and $I_{g(l)g(r)}$, are given in the right. The $I_{b(l)b(r)}$ and $I_{r(l)r(r)}$ are shifted upward by 10 and 20 μA, respectively, for clarity.

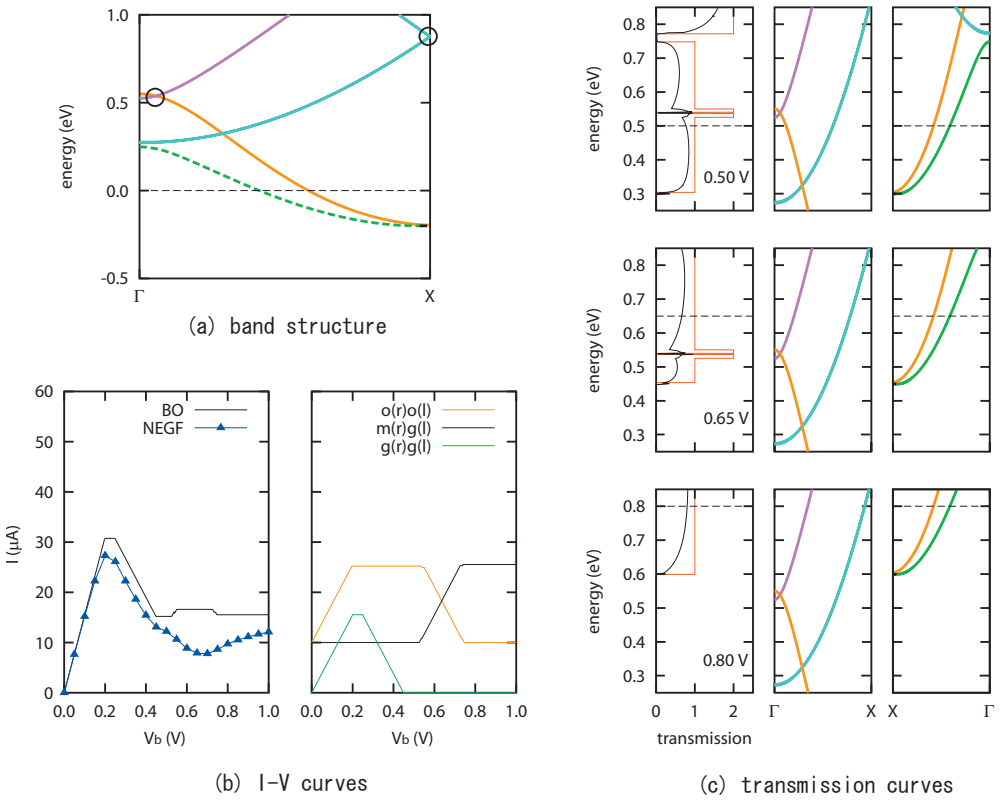

FIG. 10. (Color) Band-overlapping model for Na-doped Si_{20}-linked NW. (a) band structure near the Fermi energy. The energy is measured from the Fermi energy shown by the horizontal dashed line. The σ band is drawn by the dashed line. The green and black dashed lines are the $\sigma_{\Gamma B}$ and σ_{BX} bands, respectively. (b) I-V_b curves. The curves obtained by the BO model and NEGF calculation are given in the left. The contributions, $I_{o(l)o(r)}$, $I_{m(l)g(r)}$, and $I_{g(l)g(r)}$, are given in the right. The $I_{o(l)o(r)}$ and $I_{m(l)g(r)}$ are shifted upward by 10 μA for clarity. (c) Transmission curves, band structures of the left electrode, and band structures of the right electrode are given in the left, middle, and right, respectively. The energy is measured from the chemical potential of the left electrode μ_l. The chemical potential of the right electrode μ_r is shown by the dashed line. The results of 0.50, 0.65, and 0.80 V are given in the upper, middle, and lower rows, respectively. The transmission curves obtained by the BO model and NEGF calculation are shown by the red and black lines, respectively.

pairs. All the contributions do not reach current-decreasing region, because the band widths of the r, b, and g bands are larger than 1 eV. The dips around 0.625 and 0.925 V stem from the energy gaps indicated by red (0.028 eV) and green (0.018 eV) circles in Fig. 9(a), respectively. We note that there are other energy gaps in the regions enclosed by black circles. However, these energy gaps are negligibly small, and do not affect the overall shape of the I-V_b curve.

The I-V_b curve of the Na-doped Si_{20}-linked NW shows an up-down-up behavior as the Na-doped Si_{16}-linked NW. However, our analysis with a BO model shows that the mechanisms are somewhat different. The up-down-up I-V_b curve of the Na-doped Si_{16}-linked NW mainly stems from the increase and decrease in band-overlapping regions. On the other hand, in addition to the band overlapping, the bias dependence of scattering effect plays a key role in the Na-doped Si_{20}-linked NW.

In order to better understand the I-V_b curve, we use a BO model. By carefully comparing the transmission curve and the band structures of the left and right electrodes at bias voltages from 0 to 1 V, we find that only the green (g), orange (o), and magenta (m), and black-dashed bands contribute to the transmission curve in the transport energy range [Fig. 10(a)]. We ignore the effect of the black-dashed band, because the band width is narrow and the contribution to the current is negligible. On the other hand, we take into account of the twofold-degenerated cyan (c) band to reproduce the transmission curve at 0.50 V [Fig. 10(c)]. We also find that (i) the $[g(l),m(l)][g(r)]$ and $o(l)o(r)$ pairs are allowed, and contribute to the current, (ii) the $c(l)c(r)$ and $m(l)m(r)$ pairs are allowed, but does not contribute to the transmission in the transport energy range, and (iii) the other pairs are prohibited. Note that the σ band is shown by the dashed line. The g band is part of the σ band from the Γ point to the B point ($\sigma_{\Gamma B}$), where the B point corresponds to the bottom of the σ band. The black-dashed band is the σ_{BX} band.

Figure 10(b) compares the I_{NEGF}-V_b curve with the I_{BO}-V_b curve. The curves are qualitatively the same below 0.449 V, so that the changes in the I_{NEGF} are explained by the changes in band-overlapping regions. However, the curves differ above 0.449 V. Actually, the I_{NEGF} first decreases, and then increases. On the other hand, the I_{BO} is almost constant, except for small changes. Note that the almost constant I_{BO} occurs because the decrease in the $I_{o(l)o(r)}$ cancels out the increase in the $I_{m(l)g(r)}$ pairs. The difference between the I_{NEGF} and I_{BO} stems from the assumption that we ignore the scattering. Actually, Fig. 10(c) shows that the T_{NEGF} is quali-

tatively reproduced by the T_{BO}, but the T_{NEGF} is considerably lower than the T_{BO}. The effects of scattering first increase above 0.449 V, then decrease. This is the reason why the I_{NEGF} changes even though the effects of band-overlapping are almost constant.

IV. SUMMARY

Si-fullerene-linked NWs have the unique cage structure which is distinct from the diamond structure of bulk Si. Our first-principles calculations have demonstrated that the electronic transport properties of hydrogen terminated Si_{16}- and Si_{20}-linked NWs can be tuned by the guest-atom encapsulation. The guest-free NWs are semiconductors, and do not conduct electricity in the range of bias voltage from −1 to 1 V. The iodine or sodium doping improves the transport properties, and makes the nanowires metallic. The current in the junctions of I-doped and Na-doped NWs travels through the boundary by quantum tunneling. More significantly, the junctions have asymmetric *I-V* curves, which could be used as rectifier. The current-voltage curves are interpreted by band-overlapping models. Tunable electronic transport properties of silicon-fullerene-linked nanowires could find many applications such as field-effect transistors, conducting wires, and tunnel diode.

ACKNOWLEDGMENTS

K.N. wish to thank T. Ikeshoji for fruitful discussions. This work is supported in part by the New Energy and Industrial Technology Development Organization (NEDO) and the Next Generation Super Computing Project, the Nanoscience Program. T.O. is partly supported by CREST-JST.

APPENDIX A: CLASSIFICATION IN I-DOPED Si_{16}-LINKED NW

We classify the pairs of bands into allowed or prohibited pairs for the BO model of the I-doped Si_{16}-linked NW. We first focus on the transmission at 0 V. The eigenstates of the (left electrode)-(scattering region)-(right electrode) system at 0 V are the same as those obtained by the conventional band structure calculation using the unit cell with the periodic boundary condition. Therefore, if the electron having the χ_k character is injected into one electrode, the electron transmits to the opposite electrode without being scattered in the scattering region, and the transmitted electron does not have the character other than the χ_k character. Here, χ is the band index and k is the wave vector. In this context, the symmetry of the α band of the I-doped Si_{16}-linked NW [Fig. 5(a)] with respect to the transmission property changes at the T point, and the α band can be divided into $\alpha_{\Gamma T}$ and α_{TX} bands. The $\alpha_{\Gamma T}(l)\alpha_{\Gamma T}(r)$ and $\alpha_{TX}(l)\alpha_{TX}(r)$ pairs contribute to the transmission; so that, the pairs are allowed. On the other hand, the $\alpha_{\Gamma T}(l)\alpha_{TX}(r)$ and $\alpha_{TX}(l)\alpha_{\Gamma T}(r)$ pairs do not contribute to the transmission even though the bands overlap each other in energy; so that, the pairs are prohibited. Similarly, the $\beta(l)\beta(r)$ pair is allowed, while the $\beta(l)\alpha_{\Gamma T}(r)$ and $\alpha_{\Gamma T}(l)\beta(r)$ pairs are prohibited.

On the basis of above selection rule, the transmission curve of 0 V [Fig. 5(c)] is explained as follows. In the energy range from 0 to $E(\beta_X)$, the transmission is 2, because each of the $\alpha_{\Gamma T}(l)\alpha_{\Gamma T}(r)$ and $\beta(l)\beta(r)$ pairs contributes to the transmission by 1. Here, $E(\beta_X)$ is the energy of the β band at the X point, 0.182 eV. In the energy range from $E(\beta_X)$ to $E(\alpha_X)$, the transmission is 1, because only the $\alpha_{\Gamma T}(l)\alpha_{\Gamma T}(r)$ pair contributes to the transmission. Here, $E(\alpha_X)$ is the energy of the α band at the X point, 0.172 eV. In the energy range from $E(\alpha_X)$ to $E(\alpha_T)$, the transmission is 2, because each of the $\alpha_{\Gamma T}(l)\alpha_{\Gamma T}(r)$ and $\alpha_{TX}(l)\alpha_{TX}(r)$ pairs contributes to the transmission by 1. Here, $E(\alpha_T)$ is the energy of the α band at the T point, 0.332 eV.

Next, we show that the transmission curve of 0.1 V [Fig. 5(c)] can be explained by the selection rule determined at 0 V. In the energy range from $[E(\alpha_X)+0.1\ \text{eV}]$ to $E(\alpha_T)$, the transmission is almost 2, because each of the $\alpha_{\Gamma T}(l)\alpha_{\Gamma T}(r)$ and $\alpha_{\Gamma X}(l)\alpha_{\Gamma X}(r)$ pairs contributes to the transmission by almost 1. In the energy ranges from $E(\beta_X)$ to $E(\alpha_X)$ and from $[E(\beta_X)+0.1\ \text{eV}]$ to $[E(\alpha_X)+0.1\ \text{eV}]$, the transmission is almost 1, because only the $\alpha_{\Gamma T}(l)\alpha_{\Gamma T}(r)$ pair contributes to the transmission. In the energy range from 0 to $E(\beta_X)$, the transmission is almost 2, because each of the $\alpha_{\Gamma T}(l)\alpha_{\Gamma T}(r)$ and $\beta(l)\beta(r)$ pairs contributes to the transmission by almost 1. The $\alpha_{\Gamma T}(l)$ and $\beta(l)$ bands overlap with some of the black bands of the right electrode below 0.1 eV. However, the transmission is almost constant below 0.1 eV whether the $\alpha_{\Gamma T}(l)$ and $\beta(l)$ bands overlap with the black bands or not. From this result, we find that the pairs of the $\alpha_{\Gamma T}(l)$ band and the black bands are prohibited. The pairs of the $\beta(l)$ band and the black bands are prohibited as well. In the same way, by comparing the transmission curve and the band structures from 0 to 1 V, we find that all the black bands do not contribute to the transmission in the transport energy range. In the energy range from $E(\alpha_X)$ to $[E(\beta_X)+0.1\ \text{eV}]$, where the $\alpha_{\Gamma T}(l)$ and $\alpha_{TX}(l)$ bands overlap with the $\alpha_{\Gamma T}(r)$ and $\beta(r)$ bands, respectively, the transmission is almost 2. Since the $\alpha_{\Gamma T}(l)\alpha_{\Gamma T}(r)$ pair contributes to the transmission by almost 1, the rest of the contribution comes from the $\alpha_{TX}(l)\beta(r)$ pair. Therefore, the $\alpha_{TX}(l)\beta(r)$ pair is allowed. The symmetry of the α_{TX} band with respect to the transmission property is the same as that of the β band so that we continually join the α_{TX} and β bands to form the blue (b) band with a small energy gap of 0.010 eV at the X point. We also refer to the $\alpha_{\Gamma T}$ band as the red (r) band.

The selection rule is summarized in terms of the r and b bands as follows. The $r(l)r(r)$ and $b(l)b(r)$ pairs are allowed, while the $r(l)b(r)$ and $b(l)r(r)$ pairs are prohibited. The black bands do not contribute to the transmission in the transport energy range. We therefore need not to take account of the effects of the black bands. By comparing the transmission curve and the band structures, we find that the transmission curve from 0 to 1 V can be explained by the selection rule determined above. Note that the effects of scattering become nontrivial at high bias voltages, and reduces the efficiency of the channels. However, the transmission curve still shows steep changes at the edges of the overlapping energy ranges of allowed pair. For example, in the transmission curve of 0.7 V, we can see a steep change at 0.079 eV, above which the $r(l)$ band overlaps with the $r(r)$ band.

APPENDIX B: CLASSIFICATION IN Na-DOPED Si_{16}-LINKED NW

We note that the BO model considerably overestimates the current above 0.5 V and the T_{NEGF} is less than half of the T_{BO} in the energy range where the transmission comes from the $[c(l),m(l)][g(r),o(r)]$ pairs [Fig. 6(c)]. This means that the scattering effects are nontrivial for the $[c(l),m(l)][g(r),o(r)]$ pairs. One might think that the BO model will reproduce the NEGF calculation better, if we assume that the $c(l)o(r)$ and $m(l)g(r)$ pairs are allowed, and that the $c(l)g(r)$ and $m(l)o(r)$ pairs are prohibited. However, this assumption is wrong. Actually, from the energies where the transmission curve of 0.25 V shows steep changes, the $[c(l),m(l)][o(r)]$ pairs should be allowed [Fig. 6(c)]. Furthermore, from the T_{NEGF} curve of 0.30 V, the $c(l)g(r)$ and $[c(l),m(l)][o(r)]$ pairs should be allowed. Consequently, only the scenario that the $[c(l),m(l)][g(r),o(r)]$ pairs are allowed and the scattering effects are nontrivial explains the shape and intensity of the $T_{\mathrm{NEGF}}(E)$.

*k-nishio@aist.go.jp

[1] Y. Cui, Z. Zhong, D. Wang, W. U. Wang, and C. M. Lieber, Nano Lett. **3**, 149 (2003).
[2] Y. Cui and C. M. Lieber, Science **291**, 851 (2001).
[3] B. Tian, X. Zheng, T. J. Kempa, Y. Fang, N. Yu, G. Yu, and J. Huang, Nature (London) **449**, 885 (2007).
[4] L. Tsakalakos, J. Balch, J. Fronheiser, B. A. Korevaar, O. Sulima, and J. Rand, Appl. Phys. Lett. **91**, 233117 (2007).
[5] E. Stern, J. F. Klemic, D. A. Routenberg, P. N. Wyrembak, D. B. Turner-Evans, A. D. Hamilton, D. A. LaVan, T. M. Fahmy, and M. A. Reed, Nature (London) **445**, 519 (2007).
[6] J.-A. Yan, L. Yang, and M. Y. Chou, Phys. Rev. B **76**, 115319 (2007).
[7] M.-F. Ng, L. Zhou, S.-W. Yang, L. Y. Sim, V. B. C. Tan, and P. Wu, Phys. Rev. B **76**, 155435 (2007).
[8] M.-F. Ng, S. Lei, L. Zhou, S.-W. Yang, and V. B. C. Tan, Nano Lett. **8**, 3662 (2008).
[9] A. Svizhenko, P. W. Leu, and K. Cho, Phys. Rev. B **75**, 125417 (2007).
[10] D. D. D. Ma, C. S. Lee, F. C. K. Au, S. Y. Tong, and S. T. Lee, Science **299**, 1874 (2003).
[11] C. Delerue, G. Allan, and M. Lannoo, Phys. Rev. B **48**, 11024 (1993).
[12] A. G. Cullis and L. T. Canham, Nature (London) **353**, 335 (1991).
[13] H. I. Liu, D. K. Biegelsen, F. A. Ponce, N. M. Johnson, and R. F. W. Pease, Appl. Phys. Lett. **64**, 1383 (1994).
[14] B. Marsen and K. Sattler, Phys. Rev. B **60**, 11593 (1999).
[15] Y. Zhao and B. I. Yakobson, Phys. Rev. Lett. **91**, 035501 (2003).
[16] R. Kagimura, R. W. Nunes, and H. Chacham, Phys. Rev. Lett. **95**, 115502 (2005).
[17] K. Nishio, T. Morishita, W. Shinoda, and M. Mikami, J. Chem. Phys. **125**, 074712 (2006).
[18] K. Nishio, T. Ozaki, T. Morishita, and M. Mikami, Phys. Rev. B **77**, 201401(R) (2008).
[19] K. Nishio, T. Ozaki, T. Morishita, W. Shinoda, and M. Mikami, Proceedings of the 10th International Conference on Ultimate Integration of Silicon, pp. 61–64 (2009).
[20] K. Nishio, T. Morishita, W. Shinoda, and M. Mikami, Phys. Rev. B **72**, 245321 (2005).
[21] J. Bai, X. C. Zeng, H. Tanaka, and J. Y. Zeng, Proc. Natl. Acad. Sci. U.S.A. **101**, 2664 (2004).
[22] T. Morishita, K. Nishio, and M. Mikami, Phys. Rev. B **77**, 081401(R) (2008).
[23] K. Nishio, T. Ozaki, T. Morishita, W. Shinoda, and M. Mikami, Phys. Rev. B **77**, 075431 (2008).
[24] S. Sirichantaropass, V. M. García-Suárez, and C. J. Lambert, Phys. Rev. B **75**, 075328 (2007).
[25] U. Landman, R. N. Barnett, A. G. Scherbakov, and P. Avouris, Phys. Rev. Lett. **85**, 1958 (2000).
[26] Z. Li, H. Qian, J. Wu, B.-L. Gu, and W. Duan, Phys. Rev. Lett. **100**, 206802 (2008).
[27] T. Ozaki, K. Nishio, H. Weng, and H. Kino, Phys. Rev. B **81**, 075422 (2010).
[28] S. Datta, *Electronic Transport in Mesoscopic Systems* (Cambridge University Press, Cambridge, England, 1997).
[29] S. Datta, *Quantum Transport: Atom to Transistor* (Cambridge University Press, Cambridge, England, 2005).
[30] L. V. Keldysh, Sov. Phys. JETP **20**, 1018 (1965).
[31] C. Caroli, R. Combescot, P. Nozieres, and D. Saint-James, J. Phys. C **4**, 916 (1971).
[32] H. Kondo, H. Kino, J. Nara, T. Ozaki, and T. Ohno, Phys. Rev. B **73**, 235323 (2006).
[33] T. Ozaki, K. Nishio, and H. Kino, Phys. Rev. B **81**, 035116 (2010).
[34] P. Hohenberg and W. Kohn, Phys. Rev. **136**, B864 (1964).
[35] W. Kohn and L. J. Sham, Phys. Rev. **140**, A1133 (1965).
[36] D. M. Ceperley and B. J. Alder, Phys. Rev. Lett. **45**, 566 (1980).
[37] J. P. Perdew and A. Zunger, Phys. Rev. B **23**, 5048 (1981).
[38] W. Y. Kim and K. S. Kim, Nat. Nanotechnol. **3**, 408 (2008).
[39] M. Brandbyge, J.-L. Mozos, P. Ordejón, J. Taylor, and K. Stokbro, Phys. Rev. B **65**, 165401 (2002).
[40] T. Ozaki, Phys. Rev. B **75**, 035123 (2007).
[41] P. E. Blöchl, Phys. Rev. B **41**, 5414 (1990).
[42] N. Troullier and J. L. Martins, Phys. Rev. B **43**, 1993 (1991).
[43] T. Ozaki, Phys. Rev. B **67**, 155108 (2003).
[44] T. Ozaki and H. Kino, Phys. Rev. B **69**, 195113 (2004).
[45] J. M. Soler, E. Artacho, J. D. Gale, A. García, J. Junquera, P. Ordejón, and D. Sánchez-Portal, J. Phys.: Condens. Matter **14**, 2745 (2002).
[46] R. Landauer, IBM J. Res. Dev. **1**, 223 (1957).
[47] The code, OPENMX, pseudoatomic basis functions, pseudopotentials are available on a web site (http://www.openmx-square.org/).
[48] L. Esaki, Phys. Rev. **109**, 603 (1958).
[49] L. Esaki, Rev. Mod. Phys. **46**, 237 (1974).